High-Resolution Waveguide Terahertz Spectroscopy of Partially Oriented Organic Polycrystalline Films

Joseph S. Melinger,*,† N. Laman,‡ S. Sree Harsha,‡ ShuFan Cheng,† and D. Grischkowsky*,‡

U.S. Naval Research Laboratory, Washington, District of Columbia 20375, School of Electrical and Computer Engineering, Oklahoma State University, Stillwater, Oklahoma 74078

Received: June 26, 2007; In Final Form: August 22, 2007

We have characterized the terahertz (THz) vibrational spectroscopy of organic polycrystalline thin films using the new experimental technique of waveguide terahertz time domain spectroscopy (waveguide THz-TDS). The organic materials used in this study are tetracyanoquinodimethane (TCNQ) and 1,3-dicyanobenzene (13DCB). For each material, a thin film is cast onto one of the inner surfaces of a metal parallel plate waveguide (PPWG), followed by measurement of the low-frequency vibrational spectrum using waveguide THz-TDS. The vibrational spectra of the waveguide films are compared to corresponding vibrational spectra of standard pellet samples made by dispersing the organic solid in transparent polyethylene. We show how the waveguide films produce significantly narrower THz vibrational line shapes and reveal additional spectral lines that are obscured by inhomogeneous broadening effects in the pellet samples. When TCNQ waveguide films are cooled to 77 K, vibrational line widths as sharp as 25−30 gigahertz (0.83−1.0 cm^{-1}) at the full width at half-maximum are observed, which are among the narrowest far-infrared line widths measured for this material. The origin of the line-narrowing effect for the waveguide films is the suppression of inhomogeneous broadening due to the planar ordering of the film on the waveguide surface. The TCNQ waveguide films are further characterized using optical microscopic evaluation to understand how film morphology affects the THz vibrational spectrum. X-ray diffraction is used to determine the orientation of the polycrystalline TCNQ films on the PPWG surface and to qualitatively explain the different vibrational line strengths observed for the ordered waveguide film relative to the random pellet.

Introduction

The terahertz (THz) region from 0.1 to 10 THz (3.3−333 cm^{-1}) contains a wealth of information regarding low-frequency vibrational motion of molecular materials, ranging from the intramolecular motions of relatively small organic molecules to complex collective vibrational motion of large biological molecules such as polypeptides and DNA. The ability to resolve the complex spectra that often occur in the far-infrared for condensed phase materials is crucial to extracting useful vibrational information. This complexity is due in part to the global nature of low-frequency molecular vibrations, which can be strongly affected by intermolecular interactions such as van der Waals forces and hydrogen bonding.[1]

For condensed phase materials, homogeneous and inhomogeneous line broadening mechanisms often play a major role in obscuring the rich vibrational structure in the THz region. This is particularly true for large biomolecules where the large density of states and inhomogeneous broadening lead in most cases to featureless THz spectra.[2−4] Line broadening and spectral congestion in the THz region are often less severe for molecular solids consisting of small to medium size molecules in single-crystal form[5,6] or in polycrystalline form.[7−9]

A standard method for characterizing THz vibrational spectra involves making pellet samples whereby a polycrystalline analyte is dispersed in a transparent matrix material such as polyethylene and the mixture pressed into a pellet. Alternatively, a "thick" film of the pure analyte may be deposited on the surface of a transparent material. In some cases, these methods produce relatively sharp vibrational lines of a few wavenumbers at the full width at half-maximum (fwhm).[7,9−11] In other cases, however, randomly oriented pellet and thin films samples contain a high degree of inhomogeneous line broadening, which can severely limit the resolution of closely spaced lines even when the samples are cooled to cryogenic temperatures.[12−20] In general, one expects to observe solid-phase THz vibrational spectra with the highest degree of spectral resolution from single crystals with a minimum of defects so that inhomogeneous broadening effects are minimized.

Recently, we introduced a new technique based on the use of a single-mode parallel plate waveguide (PPWG), which demonstrated the potential to characterize the low-frequency vibrational modes of polycrystalline thin organic films with significantly higher spectral resolution than corresponding free-space measurements of (random) pellet samples of the same material.[14] The technique, called waveguide terahertz time domain spectroscopy (waveguide THz-TDS) involves the preparation of a thin polycrystalline organic film on one of the surfaces of the PPWG followed by its measurement using the standard method of THz-TDS. The PPWG consists of two parallel metal plates that are held together while maintaining a narrow gap (typically about 50 μm) over the length of the plates. The PPWG is an ideal structure for spectroscopy measurements because of the nondispersive and low-loss propagation of the transverse electromagnetic mode.[21−23] In addition, the strong

* Corresponding author. E-mail: joseph.melinger@nrl.navy.mil (J.S.M.); grischd@ceat.okstate.edu (D.G.).
† U.S. Naval Research Laboratory.
‡ Oklahoma State University.

10.1021/jp074975i CCC: $37.00
Published on Web 10/11/2007

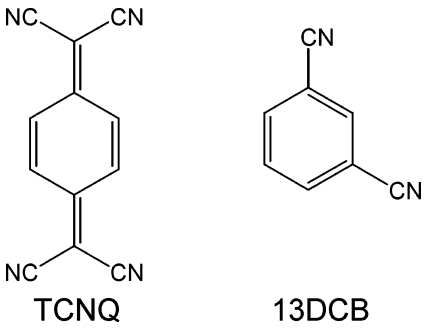

Figure 1. Chemical structures of TCNQ and 13DCB.

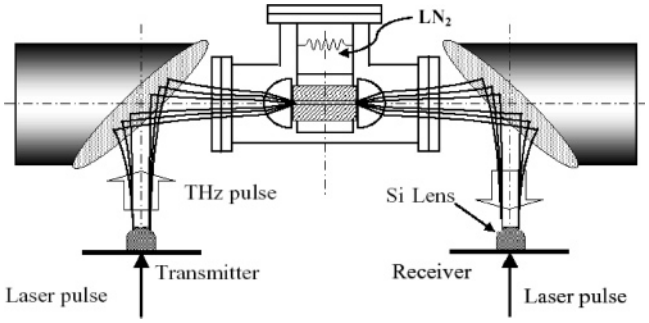

Figure 2. Schematic of the experimental apparatus for waveguide THz-TDS.

confinement of the THz wave over a relatively long propagation length (several centimeters) produces a sensitivity enhancement proportional to the ratio of the waveguide path length to the 50−100 μm separation between the plates.[21] The high sensitivity of the PPWG has been demonstrated by the detection of nanometer-thick water layers.[23]

For our experimental conditions, a substantial sensitivity enhancement is predicted for waveguide measurement of a thin film compared to the traditional single pass through the same film thickness. For a PPWG of length L and plate separation of b, the sensitivity enhancement is given by $\Gamma = L/(n^3 b)$, where n is the refractive index of the film.[21] If we take $n = 1.7$, typical for organic solids at THz frequencies and using our values of $b = 50$ μm and $L = 30.5$ mm, then $\Gamma = 124$. This high value is consistent with the nearly 2 orders of magnitude smaller quantity of sample in the waveguide film compared to the pellet for similar absorption strengths observed for the pellet and waveguide samples.[14] Note that for the study of single molecular layers or chains with n effectively unity and for our conditions, the extremely large sensitivity enhancement of $\Gamma = 610$ would be predicted.

For the small to medium size organic molecules that we have studied, molecular films are formed simply and effectively by drop-casting onto the PPWG surface from an appropriate solvent.[14,24] Other methods such as spin-casting and sublimation may also be used to produce a film on the PPWG surface. These methods result in microcrystals that are randomly oriented on the PPWG surface, but with significant planar ordering with respect to the surface. In our initial study, we compared the THz vibrational responses for a polycrystalline waveguide film and conventional pellets for the organic solid 1,2-dicyanobenzene (12DCB) and found that the waveguide THz spectra produced vibrational line widths as much as five times sharper than those found in the pellet sample.[14] In addition, the waveguide film resolved vibrational lines that were obscured by line broadening effects, thus resulting in a more informative THz vibrational spectrum.[14]

In this paper, we provide an in-depth characterization of the waveguide THz-TDS method while extending the technique to the organic solids 7,7,8,8-tetracyanoquinodimethane (TCNQ) and 1,3-dicyanobenzene (13DCB), an isomer of the previously studied 12DCB. The chemical structures of TCNQ and 13DCB are shown in Figure 1. TCNQ is a well-known organic electron acceptor used in charge-transfer crystals.[25] The DCBs have been used as precursors in the synthesis of phthalocyanines.[26] For both of these materials, we demonstrate a significant line-narrowing effect for the waveguide film relative to a pellet sample where the analyte is dispersed in a polyethylene matrix. For TCNQ, the line narrowing of the waveguide film is particularly dramatic when cooled to 77 K, which results in a well-resolved spectrum with the narrowest vibrational lines exhibiting fwhm widths in the range of 30 GHz (1.0 cm^{-1}). We believe that the TCNQ line widths measured by waveguide THz-TDS are among the narrowest far-infrared line widths measured for this material and display fwhm line widths similar to low-frequency Raman-active modes in TCNQ single crystals.[27,28]

An important goal of this study is to better understand how the morphology of the waveguide film affects the measured THz vibrational spectrum. Thus we explore different methods of producing waveguide films and attempt to correlate the observed THz responses with film morphology and as revealed by optical micrographs. In addition, we characterize the orientation of the waveguide films using X-ray diffraction and qualitatively explain the different relative vibrational line strengths observed for the waveguide film relative to the random pellet sample.

Experimental

The THz-TDS technique has previously been described in detail.[29] In its original configuration, THz-TDS comprises a pair of photoconductive antennae acting as a THz source and detector, gated by an ultrafast laser pulse (see Figure 2). The output of a titanium sapphire laser oscillator is attenuated to about 10 mW and tightly focused to gate a GaAs transmitter chip and a silicon-on-sapphire or LT-GaAs receiver chip. High-resistivity silicon lenses are used to collimate the generated THz radiation and focus it onto the receiver chip. This configuration generates a stable THz pulse train, with bandwidths extending from 100 GHz to 5 THz. For free-space measurements, the sample is placed midway between collimating parabolic mirrors. The THz pulse transmitted through the sample is time-gated by an ultrafast laser pulse, and the transient signal is Fourier-analyzed to yield the frequency-dependent absorption (and dispersion). An instrumental resolution of about 1 GHz (0.033 cm^{-1}) can be achieved.

The modifications to THz-TDS necessary for waveguide THz-TDS are shown in Figure 2. The PPWG assembly consists of two aluminum (Al) or copper (Cu) plates with identical dimensions of 27.9 mm (width) × 30.5 mm (length) × 9.5 mm (thickness). The waveguide surfaces are fabricated using standard machine-shop tolerances and are used either "as fabricated" or after polishing the inner waveguide surface to a mirror finish. A 50 μm separation between the plates is maintained by placing four 50 μm spacers at the corners of the waveguide plate. Other plate separations between 25 and 100 μm can be easily achieved using the appropriate spacer thickness. The THz beam is coupled into and out of the waveguide using high-resistivity planocylindrical silicon lenses at the input and output faces of the waveguide assembly. The polarization of the THz field is normal to the PPWG surface.

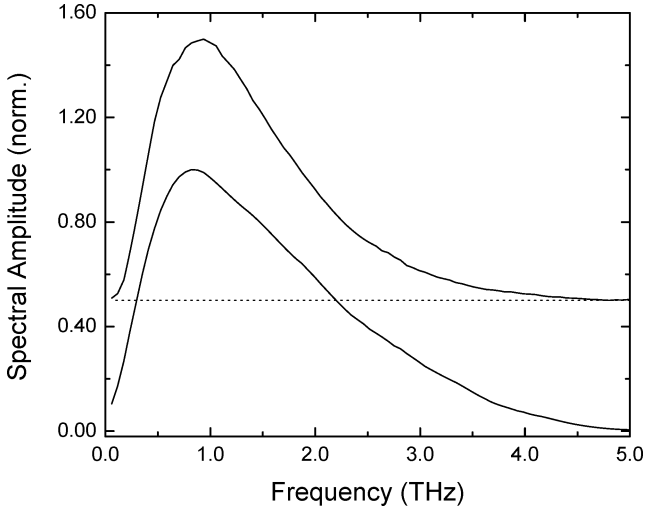

Figure 3. Comparison of typical experimental THz spectral amplitudes used in free space measurements (bottom curve) and after passage through empty waveguide (top curve, shifted up by 0.5 for clarity). Both curves are normalized to unity. The peak of the transmitted spectrum through the waveguide is typically $^1/_5$ that of the free space spectrum.

For THz experiments at 77 K, the waveguide assembly is placed inside of a vacuum chamber with straight-through optical access and mechanically attached to the surface of a liquid nitrogen container. The temperature of the waveguide is monitored by measuring the change of the temporal delay due to the temperature-dependent refractive index of the Si lenses.[30] Typical transmission efficiency of free-space THz pulses through the PPWG with a 50 μm gap is about 20% without the vacuum chamber and, due to reflections from the silicon windows, the amplitude transmission efficiency is reduced to about 10% with the chamber. Figure 3 shows typical THz spectral amplitudes corresponding to a free-space wave (bottom curve) and a wave coupled through a Cu PPWG with a 50 μm gap (top curve). In each case, a smoothly varying spectral profile is seen. Note that the spectral amplitude coupled through the empty waveguide contains useful frequency components to beyond about 4.0 THz.

The THz signal is detected using a dual-phase lock-in amplifier with a 100 ms time constant. The signal-to-noise (S/N) ratio depends critically on laser stability. For the most stable laser operation, only a single waveguide THz-TDS scan is needed for acceptable S/N levels. In some cases, up to six scans were averaged for acceptable S/N levels.

TCNQ and 13DCB were purchased from Aldrich and used without further purification. Polycrystalline thin films of TCNQ were made by drop-casting, spin-casting, and by sublimation. The drop- and spin-cast films were made using solute concentrations between 1.0 and 5.0 mg/mL in acetone. For 13DCB, the drop cast films were made from 2.0 mg/mL toluene solutions. When drop-casting, typically 150−200 μL of solution were placed onto the inner surface of one metal plate of an opened PPWG (Al or Cu). Following evaporation, the relatively thick areas of the film along the perimeter were removed using a solvent soaked swab to leave a visually uniform film on the center of the waveguide surface. The mass of the films is estimated to be approximately 100 μg for TCNQ and approximately 60 μg for 13DCB. Films made on Al and Cu surfaces yielded visually similar film morphologies. For sublimation films, an Al waveguide plate was mounted onto the cold finger of a sublimation jar a few centimeters above a small quantity of TCNQ powder placed at the bottom of the jar. The sublimation jar was then evacuated and the bottom heated to induce sublimation onto the waveguide surface.

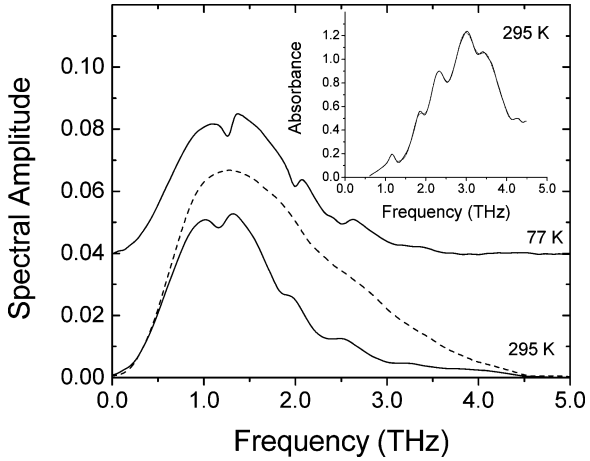

Figure 4. THz transmission spectra for a TCNQ/polyethylene pellet at 295 K (bottom curve) and at 77 K (top curve, shifted up by 0.04 for clarity). The reference pellet spectrum at 295 K is shown by a dashed line. Inset: Absorbance spectrum at 295 K obtained by normalization to the reference polyethylene pellet. The dashed absorbance line is a fit to a sum of Gaussian line shapes.

Pellet samples were prepared by mixing either TCNQ powder or 13DCB powder with polyethylene powder (Micropowders) in a ratio of about 1:10 by weight, analyte:polyethylene. The mixture was then pressed into a 13 mm diameter pellet with a thickness of 1−2 mm.

The morphology of the polycrystalline films formed on Al and Cu PPWG surfaces was characterized under a microscope at 50−100× magnification and the image recorded as an optical micrograph using a CCD camera mounted to the microscope. Because the film morphology for TCNQ and 13DCB on a glass substrate was found to be quite similar to the morphologies on Al or Cu surfaces, the crystalline order of the films was assessed by preparing films on a glass slide and inspecting the transmission pattern through the films with a polarization microscope. The orientation of drop-cast TCNQ films on Al and glass surfaces was determined by measuring the reflected X-ray diffraction pattern in the $\theta-2\theta$ mode using a Philips X'Pert diffractometer with Cu Kα radiation (1.54184 Å).

Results and Discussion

Figures 4 and 5 show THz transmission spectra at 295 and 77 K for pellet samples of TCNQ and 13DCB, respectively. For each material, the amplitude absorbance spectrum at 295 K is shown in the inset, which is obtained by normalization to a reference pellet of pure polyethylene and plotting $-\ln|A_S(\omega)/A_R(\omega)|$, where $A_S(\omega)$ and $A_R(\omega)$ are Fourier transform amplitudes of the signal pulse and reference pulse, respectively. Spectral data, including line frequencies and line widths, are collected in Table 1 and are derived either by performing nonlinear least-square fits of the absorbance spectra (as described below) or by direct estimation from the experimental spectra.

The TCNQ spectra at 295 K show a series of partially resolved vibrational lines between 1.0 and 4.5 THz. A nonlinear least-squares fit to the absorbance spectrum (Figure 4 inset) was performed using a sum of Gaussian line shapes with independent variation of the line frequency, line width, and line intensity, and yields seven lines with fwhm line widths ranging from 0.18 to 0.75 THz (6.0−25.0 cm^{-1}). When the pellet is cooled to 77 K, the lines in the transmission spectrum undergo only a moderate sharpening. A reference transmission spectrum of a neat polyethylene reference pellet was not taken at 77 K, thus

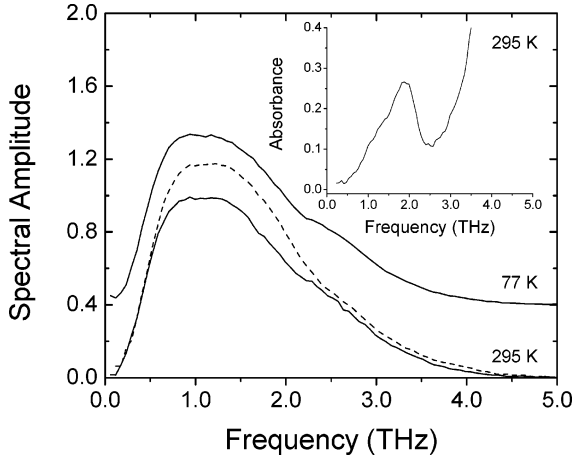

Figure 5. THz transmission spectra for the 13DCB/polyethylene pellet at 295 K (bottom curve) and at 77 K (top curve, shifted by 0.4 for clarity). The reference pellet spectrum at 295 K is shown by a dashed line. Inset: Absorbance spectrum at 295 K obtained by normalization to a reference polyethylene pellet.

TABLE 1: Line Frequencies, Line Widths, and Relative Intensities for TCNQ in a Mixed Pellet, and as a Waveguide Film[a]

	295 K			77 K			
	ν	$\Delta\nu$	I	ν	$\Delta\nu$	I	δ
TCNQ pellet	1.16	0.18	1	1.27	0.12		0.11
	1.83	0.38	4.7	1.99	0.18		0.16
	2.28	0.43	8.3	2.50	0.27		0.22
	2.97	0.75	13.3	3.04	0.50		
	3.47	0.32	2.3				
	3.70	0.60	7				
	4.31	0.35					
TCNQ film	1.20	0.08	1	1.28	0.03	1	0.08
	1.87	0.10	0.79	2.02	0.04	0.93	0.15
	2.36	0.20	1.5	2.56	0.07	1.6	0.20
	3.13	0.27	8.0	3.24	0.11	3.9	0.11
	3.46	0.34	11.8	3.44	0.13	2.9	
				3.61	0.11	7.1	
				4.41	0.08	3.8	

[a] Estimated experimental uncertainties for the line widths and line frequencies are ±10% and ±1%, respectively. ν = Line frequency in THz. $\Delta\nu$ = fwhm line width in THz. I = Relative line intensities normalized to intensity of the lowest-frequency line. δ = Frequency increase in THz upon cooling the sample from 295 to 77 K.

the fwhm line widths in Table 1 are estimated from the transmission spectrum. The vibrational line near 2.0 THz sharpens by approximately a factor of 2 relative to its value at 295 K, while the other lines sharpen by approximately a factor of 1.5. The observed vibrational frequencies and degree of line narrowing observed upon cooling the pellet to 77 K are consistent with previous far-infrared studies of random TCNQ powder samples.[15,16,31]

The THz response for the 13DCB pellet shows less sensitivity to cooling than the TCNQ pellet. The transmission spectrum of 13DCB at 295 K is relatively featureless, and the corresponding absorbance spectrum shows only a broad feature between 1.0 and 2.5 THz, exhibiting a fwhm of about 1.0 THz (33 cm^{-1}). Beyond 3.0 THz, there is the onset of absorption due to higher-frequency vibrational transitions. The features observed here are similar to those found in a recent study of the low-frequency vibrational response of dicyanobenzenes dispersed in polyethylene pellets.[32] We note that the transmission spectrum at 77 K shows only slight narrowing of the broad feature between 1.0 and 2.5 THz, and no additional spectral features are resolved upon cooling.

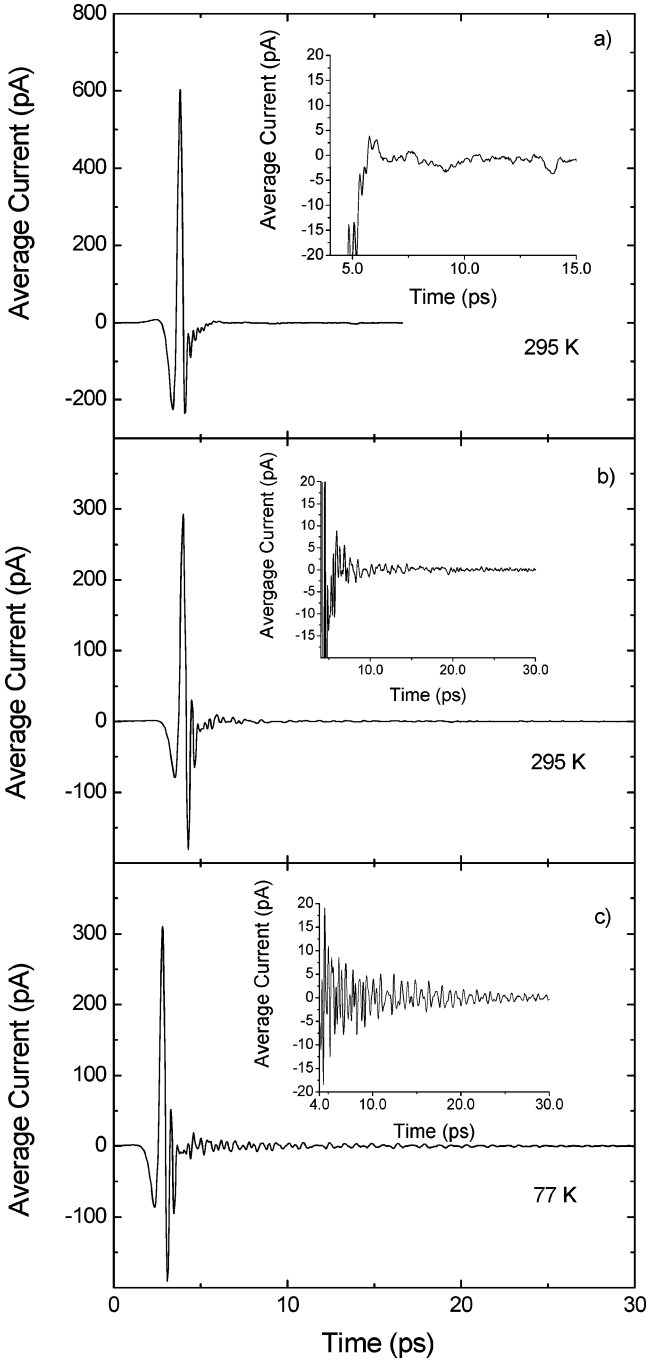

Figure 6. (a) Experimental waveguide THz-TDS pulses transmitted through an empty Cu PPWG. (b) Through the same PPWG with a drop cast TCNQ film at 295 K. (c) Through the same PPWG with a drop cast TCNQ film at 77 K. Insets: Ringing on the trailing edge of the transmitted THz pulses on an expanded vertical scale.

Waveguide THz-TDS measurements of TCNQ and 13DCB films are shown in Figures 6−10. Figure 6 compares the THz transmitted pulse through an empty Cu PPWG, and from the same PPWG containing a drop-cast TCNQ film at 295 and 77 K. The complex ringing pattern on the transmitted pulse observed for the TCNQ film is due to the beating of multiple vibrational resonances. The amplitude of the ringing pattern is enhanced and its duration lengthened when the film is cooled to 77 K. The shift to earlier times with cooling is due to the temperature-dependent refractive index of the silicon lenses.[30]

The recovery of accurate absorbance spectra is more challenging for waveguide THz-TDS because of slight changes in

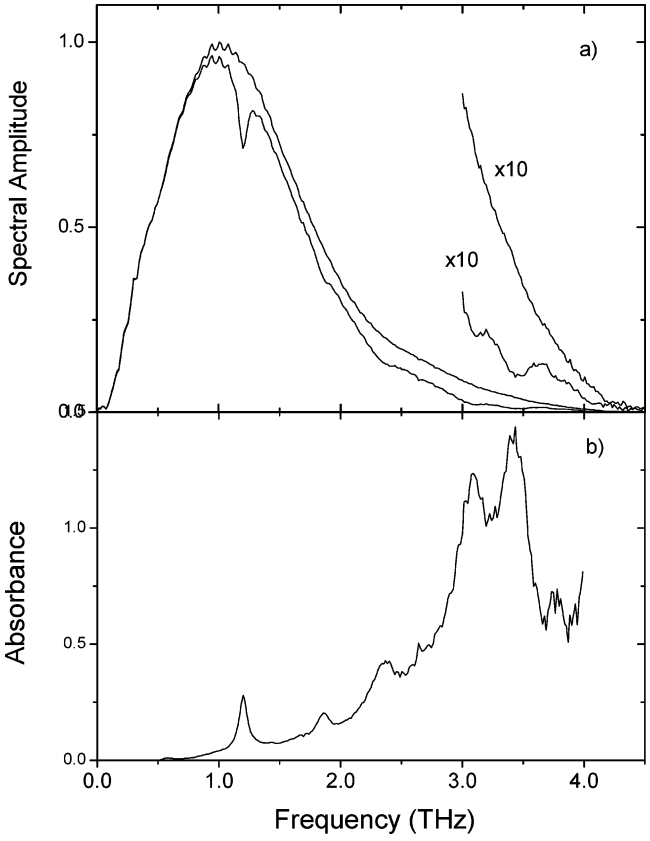

Figure 7. (a) Spectral amplitudes at 295 K for a TCNQ waveguide film in a Cu PPWG (bottom curve), and for the empty PPWG after washing away film as described in the text (top curve). (b) The resulting absorbance spectrum for the TCNQ film.

the frequency-dependent THz transmissions that occur when the PPWG is reassembled. For some films, accurate absorbance spectra at room temperature can be recovered without disturbing the waveguide by first measuring the THz transmission of the PPWG containing the film and then removing the film by rinsing with an appropriate solvent through the open access on the side of the assembly. An example of an absorbance spectrum for a TCNQ film determined in this manner is shown in Figure 7. The spectrum shows that the vibrational lines lie on top of a broad background absorption, which is noticeably reduced upon cooling to 77 K. In general, the transmitted signal increases upon cooling, implying that the background absorption is reduced. Here, it is important to note that the transmitted THz spectra through bare Al or Cu waveguides does not increase upon cooling to 77 K from room temperature.[30]

The recovery of absorbance spectra at 77 K is more challenging and is not presented here. For the remainder of the paper, we use an approximate method to determine absorbance spectra for the waveguide films. The reference transmission spectrum is estimated from the film transmission spectrum by first choosing points along the transmission profile that lie outside the absorption lines and then fitting the points with a smooth function to obtain a reference profile, which includes any broadband absorption. While this method yields only approximate line intensities, and not the broadband absorption, it is possible to extract accurate line frequencies and line widths.

At present, the measurement of the actual absorption coefficient and index of refraction of the crystals comprising the microcrystalline layer is not experimentally feasible because of the inhomogeneity of the sample layer and the lack of knowledge of the thickness of the sample layer. With respect

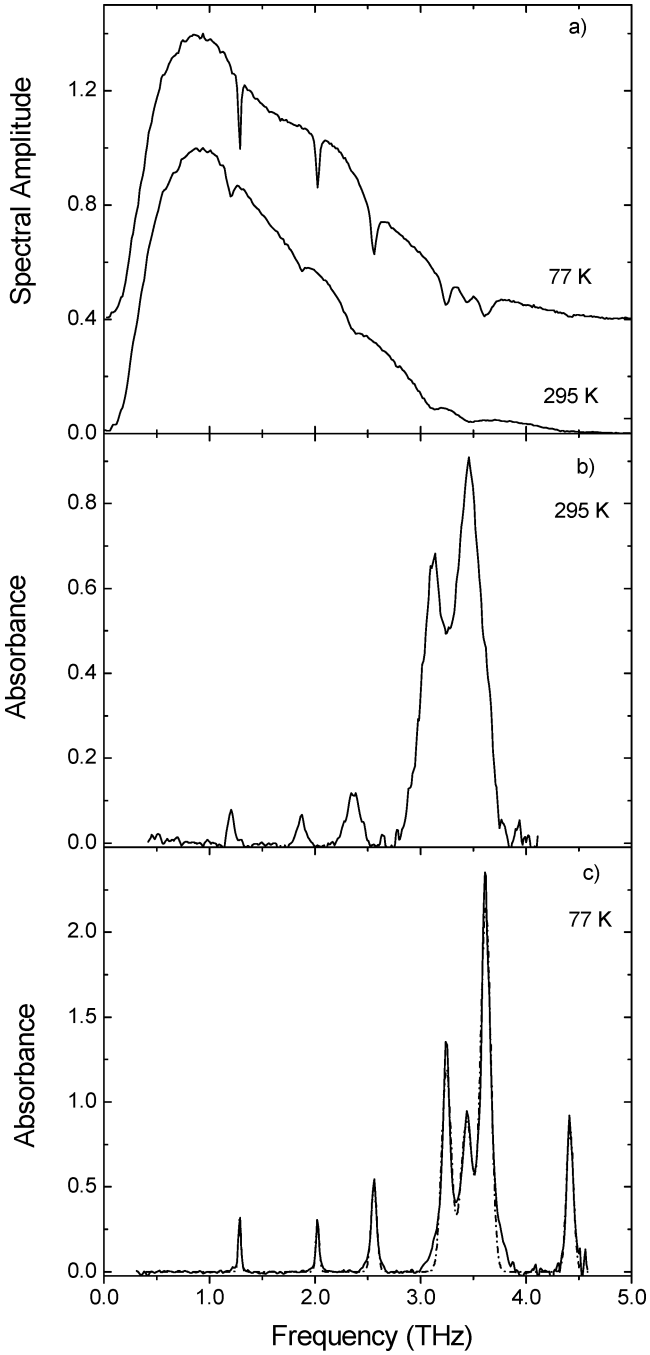

Figure 8. (a) Spectral amplitudes for a drop cast TCNQ film in a Cu PPWG. The bottom curve is measured at 295 K and the top curve at 77 K. Both spectra are normalized to unity and the 77 K spectrum is raised by 0.4 for clarity. (b) The absorbance spectrum for the TCNQ film at 295 K. (c) The absorbance spectrum for the TCNQ film at 77 K (solid), and a fit to the absorbance spectrum based on a sum of seven Gaussian line shapes (dashed line).

to the earlier waveguide THz-TDS measurement of a 20 nm homogeneous water layer, it was possible to obtain an in situ reference pulse. There, the 20 nm layer thickness was obtained by fitting the measured index to that of bulk water.[23]

Figures 8 and 10 show vibrational spectra for drop-cast films of TCNQ in a Cu PPWG and 13DCB in an Al PPWG, respectively. The waveguide films for both materials show significantly sharper vibrational lines than the corresponding pellets discussed above. In contrast to the pellet spectra, both waveguide films show pronounced line narrowing when cooled to 77 K.

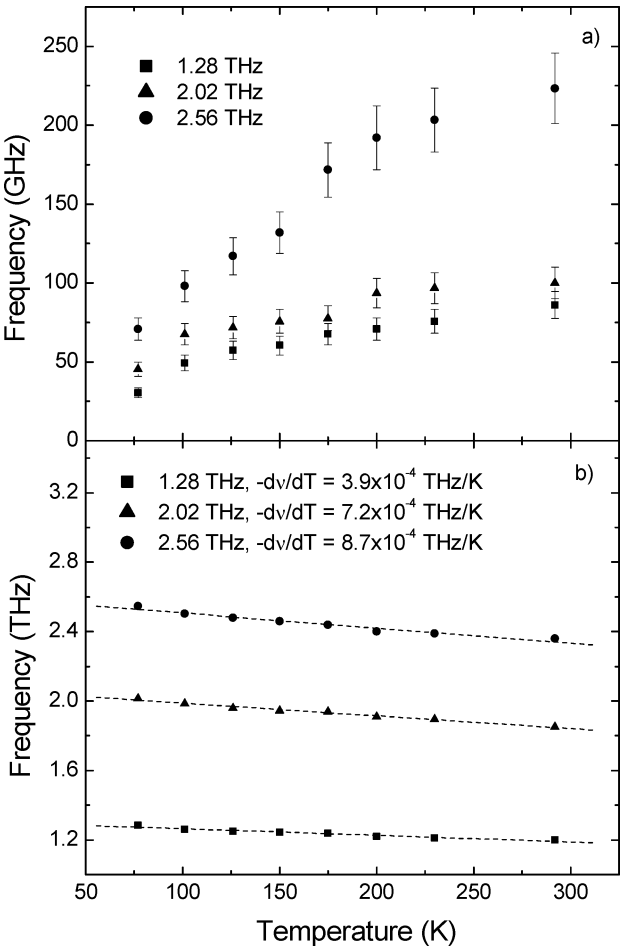

Figure 9. Temperature dependence of the fwhm line width and frequency shift for the three lowest-frequency modes observed for the TCNQ film. The indicated frequencies are given at 77 K. (a) Temperature dependence of the fwhm line width. The uncertainty in the line widths is estimated to be ±10%. (b) Temperature dependence of the frequency shift. The uncertainty in the frequencies is estimated to be ±1% (error bars not shown, but approximately represented by the size of the data points). The dashed lines represent linear fits to the data sets.

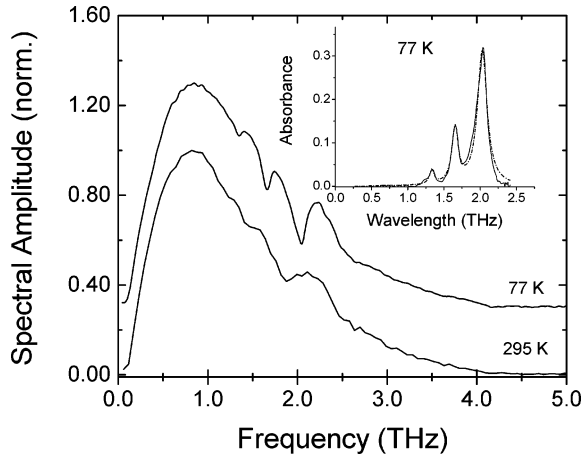

Figure 10. Spectral amplitudes for a drop cast film of 13DCB in a Al PPWG, at 295 and 77 K. Both spectra are normalized to unity and the 77 K spectrum is raised by 0.3 for clarity. Inset: The absorbance spectrum for 13DCB at 77 K (solid line), and a fit based on sum of three Lorentzian line shapes (dashed line).

For the TCNQ film, the line narrowing is particularly evident. In contrast to the TCNQ pellet (Figure 4), the three lowest-frequency vibrational bands in the waveguide film are well resolved, even at room temperature. At 295 K (Figure 8a,b), five lines are observed between 1.0 and 4.0 THz with fwhm line widths ranging between 0.08 and 0.34 THz (2.7−11.4 cm^{-1}). The line widths of the three lowest-frequency lines are approximately a factor of 2−4 times sharper than corresponding line widths for the pellet at 295 K. When the film is cooled to 77 K (Figure 8c), the vibrational lines narrow by a factor of 2.0−2.5, and the line frequencies shift to higher values. For the three lowest-frequency modes, the line frequencies at 77 K are between 6% and 8% higher than their corresponding frequencies at 295 K. The relatively high S/N achieved for the 77 K measurements clearly resolves seven vibrational lines. In particular, the relatively broad doublet between 3.0 and 4.0 THz observed at 295 K has split into three relatively sharp lines. Fits to the spectrum in Figure 8c were attempted using either a sum of Gaussian or Lorentzian line shapes. A somewhat better fit (shown in Figure 8c) is found using the Gaussian line shape, although neither profile fits the wings of the experimental line shapes particularly well. The narrowest line widths occur for the lowest-frequency lines. For example, the 1.28 THz (43 cm^{-1}) mode narrows to a fwhm width of 0.03 THz (1.0 cm^{-1}) and the 2.02 THz (67.3 cm^{-1}) mode narrows to a fwhm width of 0.04 THz (1.3 cm^{-1}), which is a narrowing of about four times relative to the corresponding lines in the pellet. In addition, the relative intensities of the vibrational lines of the waveguide film (at 295 K) are different than those of the corresponding pellet (see Table 1).

The effectiveness of waveguide THz-TDS in providing sharper spectral lines may be assessed by comparing the line widths obtained from the TCNQ waveguide films to previous measurements of the low-frequency vibrational lines of TCNQ single crystals. To our knowledge, only limited far-IR measurements covering frequencies above about 1.8 THz (60 cm^{-1}) have been performed on TCNQ single crystals at room temperature.[31,33] Spontaneous Raman measurements of vibrational line shapes have been made on single crystals of TCNQ at both room temperature and at cryogenic temperatures.[27,28] Comparing the waveguide THz-TDS measurements to the Raman measurements of refs 27 and 28 shows that waveguide THz-TDS achieves similar line widths to the single-crystal Raman measurements. For example, the Raman-active 1.23 THz (41 cm^{-1}) mode of the TCNQ single-crystal exhibit fwhm line widths of approximately 0.035 THz (1.1 cm^{-1}) and 0.09 THz (3.0 cm^{-1}) at 90 and 293 K, respectively,[27] which are quite similar to the line widths of the lowest-frequency mode of the TCNQ waveguide film measured at 77 and at 295 K (see Table 1).

The detailed temperature dependence of the line width and frequency shift for the three lowest-frequency modes given in Table 1 are plotted in Figure 9. The values for the line width and mode frequency are determined by fitting TCNQ spectra measured at each temperature to a sum of Gaussian line shapes in the manner described above. The fwhm line widths for each of the modes (Figure 9a) are observed to decrease monotonically as the film is cooled from 295 to 77 K, with the fwhm line width of the two lower-frequency modes sharpening by about a factor of 2. The fwhm of the mode at 2.56 THz displays stronger temperature dependence, narrowing by about a factor of 3 over the same temperature range. The stronger temperature dependence of the line width for this mode is likely due to a stronger coupling to thermally activated bath phonons, which results in faster vibrational energy relaxation.

The mode frequencies in Figure 9b are each observed to shift to higher frequency as the temperature is cooled to 77 K with

a nearly linear dependence. A linear fit is performed for each data set and the quantity $-\mathrm{d}\nu/\mathrm{d}T$ is recovered, where ν is the mode frequency and T is the temperature. The values of $-\mathrm{d}\nu/\mathrm{d}T$ are 3.9×10^{-4} THz/K for the 1.28 THz mode, 7.2×10^{-4} THz/K for the 2.02 THz mode, and 8.7×10^{-4} THz/K for the 2.56 THz mode. The temperature dependence of the frequency shift observed here is somewhat larger than that observed in reference 27 for Raman-active modes of TCNQ crystals in the THz region, which has values for $-\mathrm{d}\nu/\mathrm{d}T$ of 2.52×10^{-4} THz/K, 3.06×10^{-4} THz/K, and 5.76×10^{-4} THz/K for Raman-active mode frequencies of 1.23, 1.95, and 2.40 THz, respectively.

Similar distinctions between the waveguide and pellet vibrational spectra are observed for 13DCB. Figure 10 shows that the broad feature between 1.0 and 2.0 THz at 295 K begins to resolve into three lines. When cooled to 77 K, the spectrum undergoes additional sharpening and the broad feature clearly resolves into three lines. The line frequencies also shift to higher values when the film is cooled to 77 K. In contrast to the TCNQ film, a better fit to the 13DCB spectrum is found by using a sum of Lorentzian line shapes (inset, Figure 10). Here, vibrational frequencies are observed at 1.33 THz (44.3 cm^{-1}), 1.65 THz (55.0 cm^{-1}), and 2.05 THz (68.3 cm^{-1}), with corresponding fwhm line widths of 0.07 THz (2.3 cm^{-1}), 0.11 THz (3.7 cm^{-1}), and 0.16 THz (5.3 cm^{-1}). As noted above, similar resolution into three lines is not observed for the 13DCB pellet, even at 77 K.

A likely explanation for the narrower line shapes and more pronounced temperature dependence of the waveguide films is that the vibrational modes of the film contain a smaller degree of inhomogeneous broadening than do those of the corresponding pellet samples. Vibrational line shapes for molecular solids typically display a mixture of homogeneous (dynamic) and inhomogeneous (static) broadening. Homogeneous broadening mechanisms such as vibrational energy exchange and pure dephasing are temperature dependent and thus become quenched at sufficiently low temperature.[34,35] In contrast, inhomogeneous broadening, which may be produced by a static distribution of transition frequencies, is less sensitive to temperature. The pellet samples consist of a broad distribution of microcrystalline sizes that are randomly oriented in the polyethylene matrix. For the TCNQ and 13DCB pellets studied here, such disorder apparently leads to vibrational line shapes that are dominated by inhomogeneous broadening. In addition, interactions between the analyte microcrystals and the polyethylene matrix, and changes to the sample induced by preparation under high pressure, may also contribute inhomogeneous broadening.

Suppression of inhomogeneous broadening may be anticipated if the waveguide films contain a high degree of order on the PPWG surface. Indeed, a microscopic characterization of the TCNQ film that yielded the sharp vibrational lines of Figure 8c shows that it consists largely of dendritic microcrystals that are randomly oriented on the PPWG surface but exhibiting significant planar order with respect to the surface (see Figure 11a below). To confirm crystalline order, we have examined drop-cast TCNQ films with similar dendritic microcrystals on glass substrates using a polarized optical microscope. The individual microcrystals of such films exhibit essentially complete extinction of transmission, which indicates the film is composed of highly crystalline material. We suggest that the increased planar ordering of the waveguide film together with formation of high-quality microcrystals with a minimum of defects is a requirement to observe strong line-narrowing properties in waveguide films.

The detailed line shapes of the low-frequency vibrational modes are determined by the relative contributions of homogeneous and inhomogeneous broadening and anharmonicity of the molecular potentials. As noted above, the wings of the TCNQ line shapes are not well fit by either Gaussian or Lorentzian line shapes. A Voigt profile consisting of a convolution of Lorentzian and Gaussian line shapes is likely to be a more realistic description. In addition, anharmonicity can also play an important role on determining the width and shape of low-frequency vibrational lines because of the thermalized distribution of population within the vibrational ladder. For example, for a harmonic approximation of the TCNQ 1.2 THz mode at 295 K, the ratio of vibrational population in the $n = 12$ and $n = 0$ levels, or P_{12}/P_0, is 0.096. At 77 K, P_3/P_0 is 0.105. Significant positive anharmonicity leads to an asymmetric broadening of the line shape, with a tail that extends to lower frequencies.[11] We have attempted to fit the temperature dependence of the line shape for the three lowest-frequency TCNQ lines using a Morse oscillator model (not shown here). We find that anharmonicity values as much as 0.1% of the fundamental frequencies leads to significantly distorted line shapes, especially at temperatures near 295 K. Because our experimental line shapes do not show obvious tails on their low-frequency wings, we suggest that for TCNQ anharmonicity contributes a relatively small amount of line broadening relative to other sources of homogeneous and inhomogeneous broadening.

For TCNQ, we have characterized how microcrystal morphology affects the vibrational spectrum as measured by waveguide THz-TDS. Because of their collective nature, it may be expected that low-frequency vibrational modes will be sensitive to the size of the microcrystals and the degree of crystalline order. Furthermore, external modes that involve the coherent motion of many molecules are expected to show greater sensitivity to the microcrystal morphology than internal modes.

The shape of the microcrystals depends in a sensitive way on the method used to prepare the film. Microcrystals with very different shapes are formed by drop-casting, spin-casting, and sublimation. For the drop-casting method, the microcrystal morphology depends on the solute concentration. Figure 11 shows optical micrographs of representative films made by different methods and their associated waveguide THz-TDS spectra measured at 77 K. Parts a−c of Figure 11 show how the microcrystal shape depends on the solute concentration when drop-casting is used to form the film. At a relatively low TCNQ concentration (1.3 mg/mL), a dendritic structure is formed where the largest microcrystals have lengths of approximately 30 μm in the longest dimension. The corresponding vibrational spectrum is the same as in Figure 8c and is reproduced in Figure 11a for convenience. Higher TCNQ concentrations (2.4 mg/mL) lead to the formation of small rhombic plates with a distribution of sizes as shown in Figure 11b. The largest rhombs have sides of about 15−20 μm in length. Only minor changes in the vibrational spectrum are observed for this film and occur mainly in the relative intensities of the group of three lines near 3.5 THz. Figure 11c shows the morphology of a drop-cast film made from a relatively concentrated TCNQ solution of 5 mg/mL. Here, larger rhombic plates are formed with the largest microcrystals having sides more than 50 μm in length. In addition, the film also contains smaller rhombic plates and some dendritic structures. The vibrational spectrum in this case shows a considerable increase in the relative intensity of the 1.28 THz mode. This film morphology also produced the narrowest line width (fwhm = 25 GHz: 0.83 cm^{-1}) for the 1.28 THz mode, which is shown in the inset of Figure 11c. The higher-frequency

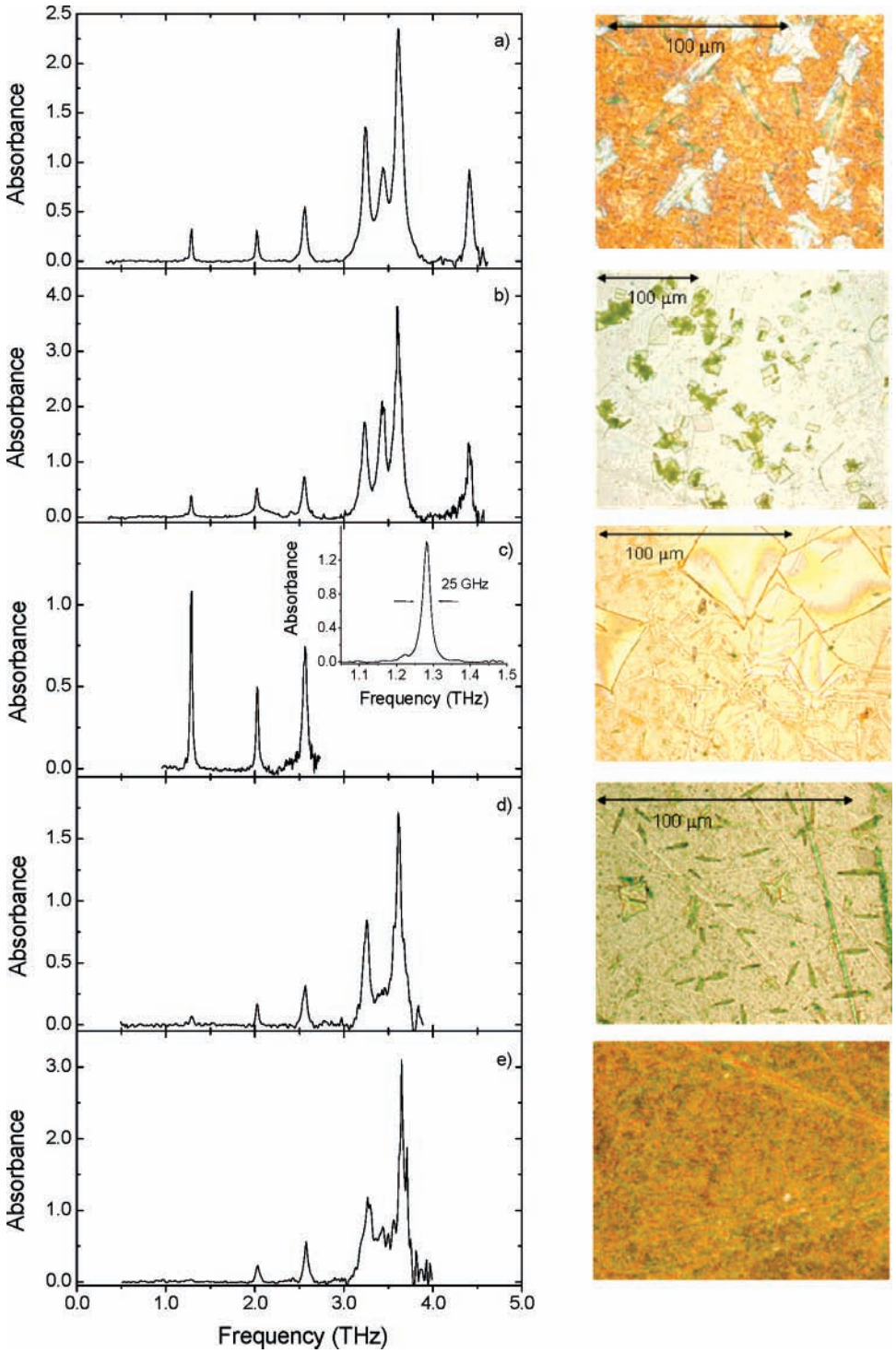

Figure 11. THz spectra for TCNQ waveguide films prepared using different methods and their corresponding optical micrographs. (a) Drop cast film for a 1.3 mg/mL TCNQ solution on Cu. (b) Drop cast film for a 2.4 mg/mL TCNQ solution on Al. (c) Drop cast film for a 5.0 mg/mL TCNQ solution on Cu. Inset: Mode at 1.28 THz on an expanded scale. (d) Spin cast film on Al from a 2.0 mg/mL solution. (e) Sublimation film on Cu. All spectra are measured at 77 K.

modes were not detected in this case because of the strong absorption of the thicker film, which required a 100 μm waveguide spacing. Significant differences in the TCNQ vibrational spectrum are observed for spin-cast and sublimation films shown in Figure 11d,e. Spin-casting (Figure 11d) produced mainly needlelike microcrystals with average lengths of about 10 μm. In addition to these, a small fraction of microcrystals have a triangular platelike shape. The most notable differences in the vibrational spectrum of spin-cast microcrystals are the reduced intensities of the 1.28 THz mode and the 3.44 THz mode with respect to the other modes. The sublimation film (Figure 11e) produced the microcrystals smaller than could be estimated using 100× magnification. The vibrational spectrum is similar to that of the spin-cast film, with the exception that the intensity of the 1.28 THz mode is almost totally attenuated.

Clearly, a wide range of microcrystal shapes and sizes may be obtained depending on the method and specific conditions of film preparation. The positions of the vibrational frequencies and their line widths appear little changed for the different morphologies shown in Figure 11, however, noticeable differ-

ences occur for the relative line intensities. In particular, the modes at 1.28 and 3.44 THz are sensitive to the size of the microcrystals. Both modes exhibit significantly weaker relative intensity for films containing the smallest microcrystals, while the 1.28 THz mode shows increased relative intensity for the largest rhomb microcrystals. This dependence on morphology suggests that these modes have substantial external vibrational character.

The formation of a film with planar ordering on the PPWG surface potentially allows polarization effects to be observed in waveguide THz-TDS. If the planar orientation of the microcrystals is known with respect to the polarization of the THz field, then, in principle, the differences observed in the relative line strengths for the waveguide film and the random pellet (due to the polarization of the vibrational modes) can aid in the assignment of the vibrational lines. TCNQ films were characterized for orientation using reflection X-ray diffractometry. This was done for drop-cast TCNQ films on both Al and glass substrates that yielded the dendritic and rhombic plate morphologies shown in parts a and b of Figure 11, respectively. For a given TCNQ solution concentration, both the Al and glass substrates produced very similar microcrystal morphologies under inspection with a microscope.

TCNQ crystallizes in the monoclinic system having space group $C2/c$ and with four molecules per unit cell.[36] The X-ray diffraction pattern observed for dendritic TCNQ microcrystals is shown in parts a (on glass) and b (on Al) of Figure 12. For both substrates, diffraction peaks due to TCNQ at $2\theta = 10.93°$, 21.94°, and 33.15° (and 44.68° for TCNQ on glass) dominate the spectrum. In Figure 12b, strong peaks at $2\theta = 38.42°$ and 44.62° are due to the Al substrate. The positions and relative intensities of the TCNQ peaks were compared to a simulated X-ray diffraction spectrum of TCNQ using Mercury[37] and are found to be consistent with diffraction from the (00l) planes of the unit cell (with $l = 2$, 4, 6, and 8). Considering the absence of strong peaks due to other TCNQ planes, the data strongly suggest that the film has a dominant orientation where the c-axis of TCNQ unit cell points upward from the substrate surface, making an angle of 8.5° with respect to the surface normal, and that the (001) plane of the unit cell is aligned parallel to the waveguide surface. Consequently, for the polycrystalline sample film, the distribution of c axes of the individual microcrystals defines a cone with an angle of 8.5° about the THz polarization. The diffraction spectrum of the film on Al shows a few relatively weak lines that are just resolvable from the baseline, which are due to other TCNQ crystal planes and which indicates that other orientations are present to a minor extent. The higher degree of roughness of the Al surface relative to the glass surface may account for more variation in microcrystal orientation.

The X-ray diffraction pattern corresponding to the rhombic plates are shown in Figure 12c,d. Here the diffraction peaks of the (00l) planes again dominate the spectrum, however, there is a somewhat stronger contribution from diffraction from other planes, particularly for the film on Al. The film of rhombic plates is cast from a relatively concentrated TCNQ solution (2.4 mg/mL), which produces a thicker film than that for the dendritic microcrystals. Partial stacking of the plates in the thicker film is likely to produce a greater fraction of microcrystals with different orientations with respect to the substrate.

A schematic of the TCNQ unit cell showing its orientation on the substrate and with respect to the experimental electric field polarization is shown in Figure 13. In addition, the molecular axes (X, Y, and Z) for an individual TCNQ molecule

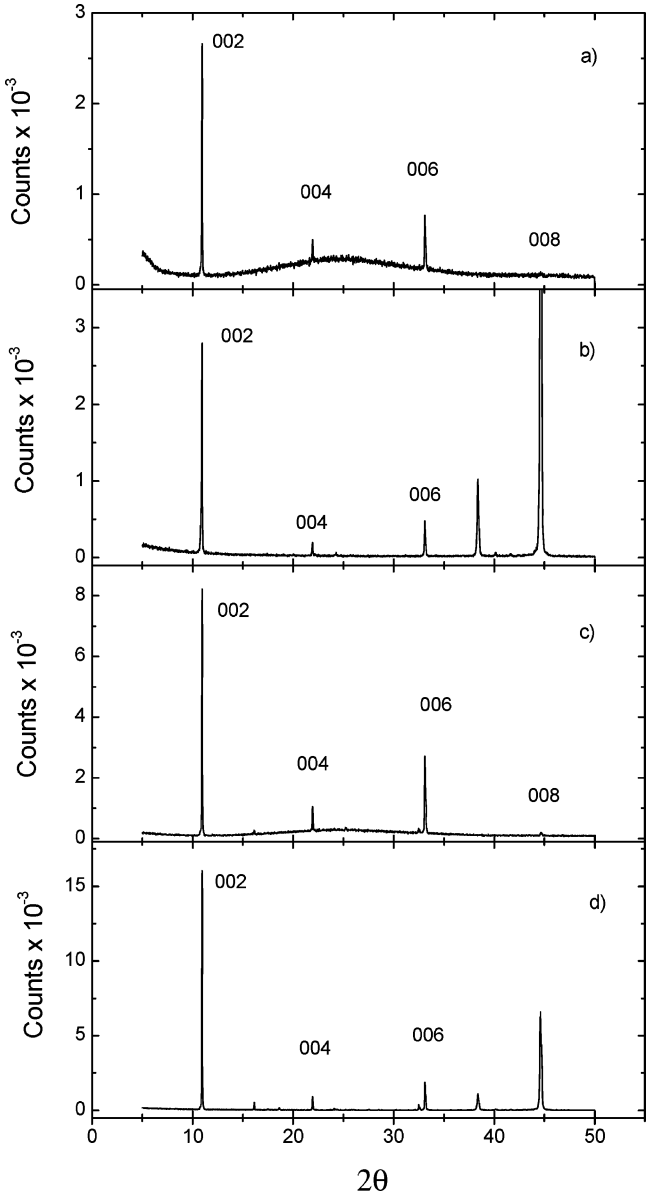

Figure 12. X-ray diffraction patterns for TCNQ films on glass and polished Al surfaces. In each panel, the major peaks due to TCNQ are assigned to crystal planes and indicated as (002), (004), and (006) (and (008) on glass). (a) Dendritic microcrystals on glass. (b) Dendritic microcrystals on Al. (c) Rhombic microcrystals on glass. (d) Rhombic microcrystals on Al. Peaks due to Al are at $2\theta = 38.42°$ and 44.62°.

are also defined. The X axis is perpendicular to the plane of the TCNQ molecule, while the Y and Z axes are in the plane and are oriented as shown. A table of proportionality factors for band intensities along the a, b, c, and c^* ($\perp ab$) axes of the unit cell is reproduced from data from ref 31. With the (001) plane aligned parallel to the waveguide surface, the a and b axes are perpendicular to each other and are in the plane of the waveguide, and the b and c axes are perpendicular. The c^* axis is parallel to the electric field polarization. In this configuration, internal vibrational modes that are polarized along the Y and Z molecular axes have greater projections along the c^* axis and are expected to show enhancement in the waveguide film. A comparison of pellet and waveguide film spectra at 295 K (Figures 4 and 8b, respectively) suggests that the vibrational mode near 3.5 THz gains relative intensity in the waveguide film spectrum, whereas modes near 1.87, 2.4, and 3.0 THz lose relative intensity. Previous experimental and theoretical inter-

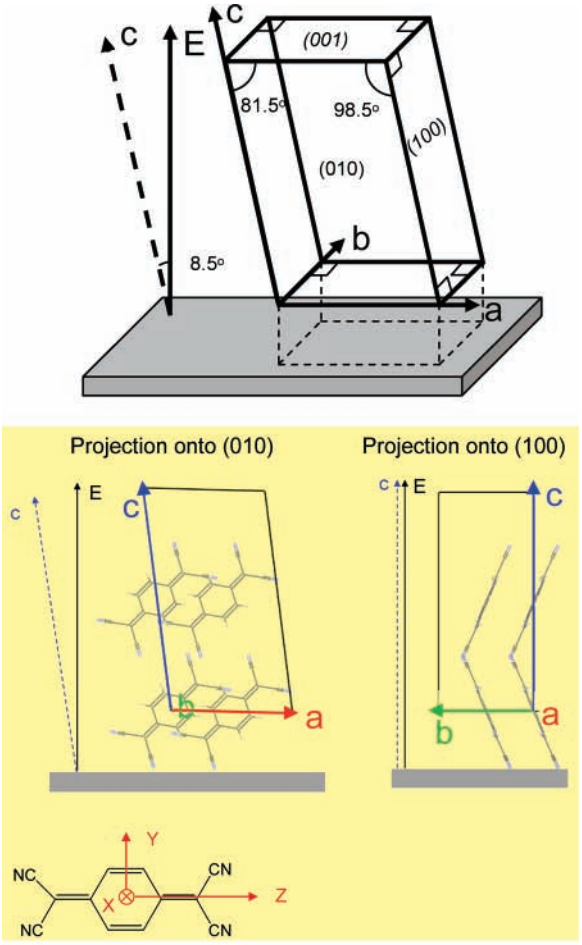

Crystal Direction	X	Y	Z
a	0.00	0.56	0.43
b	0.84	0.07	0.09
c	0.16	0.49	0.35
c* (⊥ ab)	0.16	0.35	0.49

Figure 13. Top: Schematic of the TCNQ unit cell showing its orientation on the metal PPWG surface and with respect to the experimental electric field polarization. The electric field is polarized perpendicular to the PPWG surface. Middle: Projection of the TCNQ unit cell onto the (010) plane (top, left) and (100) plane (top, right) and with respect to the experimental electric field. For the projection onto (010), the two molecules on the left have their centers at $a = 0$ and $b = 0$, while the two molecules on the right are displaced one-half of a lattice translation along *b*. The *c*-axis of the unit cell makes an angle of 8.5° with the electric field polarization vector. With the (001) plane aligned parallel to the waveguide surface, the *a* and *b* axes are perpendicular to each other and are in the plane of the waveguide, and the *b* and *c* axes are perpendicular. The molecular axes of an individual TCNQ are shown. The *X* axis is perpendicular to the plane of the TCNQ molecule, while the *Y* and *Z* axes are in the plane and are oriented as shown. The table gives the proportionality factors for band intensities along the crystal axes (data from ref 31).

pretations of the low-frequency vibrational spectrum of TCNQ differ in the assignment of the spectral lines.[16,31,33] For example, early work interprets the lowest three frequency lines as external vibrations (phonons).[31] By "external vibrations", we mean collective vibrational motion such as lattice translations and intermolecular librations, and by "internal vibration", we mean an intramolecular vibration. Other studies interpret the low-frequency modes below about 4.0 THz as having mixed internal and external character.[27,33] If we accept that the three lowest-frequency lines correspond to external vibrations, then the results above suggest that the modes at 1.87 and 2.36 THz do not have strong projections onto the *c** axis because their relative intensities are attenuated in the oriented waveguide film spectrum. Reference 31 has assigned the mode near 3.0 THz (100 cm^{-1}) to an out-of-plane ring bend (along *X*), which has a relatively weak projection onto the *c** axis, and the mode near 3.5 THz (115 cm^{-1}) as an in-plane bending of the NC−C−CN groups (along *Z*), which has a relatively strong projection onto the *c** axis. The enhancement in relative intensity in the waveguide film near 3.5 THz appears to be consistent with this assignment of internal vibrational motion. Clearly, an angle-dependent THz characterization of an oriented single TCNQ crystal would be valuable to more confidently assess polarization effects in waveguide THz-TDS.

Summary and Conclusions

In this paper we have provided an in-depth characterization of waveguide THz-TDS. The technique has been extended to the organic solids TCNQ and 13DCB. The strong line narrowing of partially oriented waveguide films relative to random pellet samples serves to generalize our original observation of line narrowing for 1,2-dicyanobenzene polycrystalline films in a PPWG.[14] For TCNQ, waveguide THz-TDS has provided unprecedented spectral resolution for the measurement of its low-frequency infrared active modes. We anticipate that further cooling from 77 to 4 K would provide an additional increase of line narrowing.

Our microscopic characterization of the waveguide films emphasizes that both planar ordering and high crystalline quality are required in order to achieve the narrowest possible lines and strongest possible line intensities. We have attributed the line narrowing effect, in part, to a reduction of inhomogeneous broadening in the waveguide films, associated with the planar ordering of microcrystals on the inner surface of the PPWG. We believe that waveguide THz-TDS will provide increased spectral resolution relative to standard free-space characterization of random samples for a variety of solids that form films with such planar order. Indeed, our recent observations of similar line-narrowing effects for waveguide films of biological molecules containing hydrogen-bonding interactions emphasizes the broad applicability of the technique.[24] In contrast, materials that form amorphous films in the PPWG may not show improved spectral resolution relative to standard methods, although a sensitivity enhancement may still be achieved relative to standard free-space characterization.

The microscopic and X-ray analyses highlight a key experimental feature of waveguide THz-TDS. The PPWG is easily opened to allow the structural properties of the film to be determined and then compared with the THz characterization. The X-ray diffraction results conclusively showed that the TCNQ film has a strong preferential orientation with the (001) plane of the unit cell parallel to the waveguide surface. The degree of orientation is related to both the flatness of the surface and the conditions of film formation. Because the THz field is highly polarized, knowledge of the film orientation may then be used to extract information about the polarization of molecular vibrations.

Waveguide THz-TDS offers an alternative method to study the low-frequency vibrational properties of organic solids. A

major strength of waveguide THz-TDS is its potential to provide THz vibrational spectra with higher spectral resolution than conventional THz characterization using random pellets. For the materials studied here, thin film sample preparation is easier than growing large single crystals and the measured line widths approach those of single-crystal data. The more precisely measured frequencies can provide more rigorous experimental data for theoretical modeling of low-frequency vibrational structure. In addition, waveguide THz-TDS requires approximately 1% of the amount of sample required for a pellet measurement. This could be further reduced to 0.1% by minimizing the waveguide spacing and increasing the waveguide length. The combination of high spectral resolution and high sensitivity suggests potential application to the detection of small quantities of unknown substances through detection of vibrational fingerprint resonances. A disadvantage of waveguide THz-TDS is an inability to make quantitative measurements of the absorption coefficient and refractive index for the noncontinuous polycrystalline films studied here. For continuous films with a known thickness inside of a PPWG, it is possible, in principle, to extract quantitative phase and absorption information.

The film preparation method of drop-casting has provided a simple and convenient way to achieve an initial degree of order in the PPWG films. In the future, we intend to explore methods to improve both the orientation and crystallinity of waveguide films. For example, recent studies have shown that an appropriately functionalized self-assembled monolayer on a metal surface can provide a template for the growth of highly oriented organic thin films.[38] Such methods could be used to grow highly oriented films on the inner surface of the PPWG and could provide additional increases in spectral resolution.

Acknowledgment. This work was supported by the Office of Naval Research and by the National Science Foundation.

References and Notes

(1) Walther, M.; Fischer, B. M.; P. Uhd Jepsen, P. *Chem. Phys.* **2003**, *288*, 261−268.

(2) Markelz, A. G.; Roitberg, A.; Heilweil, E. J. *Chem. Phys. Lett*. **2000**, *320*, 42.

(3) Brucherseifer, M.; Nagel, M.; Haring Bolivar, P.; Kurz, H.; Bosserhof, A.; Buttner, R. *Appl. Phys. Lett.* **2000**, *77*, 4049−4051.

(4) Zhang, Chenfang; Tarhan, Enver; Ramdas, A. K.; Weiner, A. M.; Durbin, S. M. *J. Phys. Chem. B* **2004**, *108*, 10077−10082.

(5) Rungsawang, R.; Ueno, Y.; Tomita, I.; Ajito, K. *J. Phys. Chem. B* **2006**, *110*, 21259−21263.

(6) Barber, J.; Hooks, D. E.; Funk, D. J.; Averitt, R. D.; Taylor, A. J.; Babikov, D. *J. Phys. Chem. A* **2005**, *109*, 3501−3505.

(7) Johnston, M. B.; Herz, L. M.; Khan, A. L. T.; Köhler, A.; Davies, A. G.; Linfield, E. H. *Chem. Phys. Lett.* **2003**, *377*, 256.

(8) Liu, H.-B.; Zhang, X.-C. *Chem. Phys. Lett*. **2006**, *429*, 229.

(9) Upadhya, P. C.; Shen, Y. C.; Davies, A. G.; Linfield, E. H. *J. Biol. Phys.* **2003**, *29*, 117−121.

(10) Walther, M.; Plochocka, P.; Fischer, P. B.; Helm, H.; Uhd Jepsen, P. *Biopolymers* **2002**, *67*, 310−313.

(11) Korter, T. M.; Plusquellic, D. F. *Chem. Phys. Lett.* **2004**, *385*, 45−51.

(12) Kutteruf, M. R.; Brown, C. M.; Iwaki, L. K.; Campbell, M. B.; Korter, T. M.; Heilweil, E. J. *Chem. Phys. Lett*. **2003**, *375*, 337−343.

(13) Walther, M.; Fischer, B.; Schall, M.; Helm, H.; Uhd Jepsen, P. *Chem. Phys. Lett*. **2000**, *332*, 389−395.

(14) Melinger, J. S.; Laman, N.; Sree Harsha S.; Grischkowsky, D. *Appl. Phys. Lett*. **2006**, *89*, 251110−251112.

(15) Futamata, M.; Morioka, Y.; Nakagawa, I. *Spectrochim. Acta, Part A* **1983**, *39*, 515−528.

(16) Takenaka, T. *Spectrochim. Acta, Part A* **1970**, *27*, 1735.

(17) Shotts, W. J.; Sievers, A. J. *Biopolymers* **1974**, *13*, 2593−2614.

(18) Lee, S. A.; Anderson, A.; Smith, W.; Griffey, R. H.; Mohan, V. *J. Raman Spectrosc.* **2000**, *31*, 891; Li, J.; Lee, S. A.; Anderson, A.; Lettress, L.; Griffey, R. H.; Mohan, V. *J. Raman Spectrosc.* **2003**, *34*, 183−191.

(19) Nishizawa, J.; Sasaki, T.; Suto, K.; Tanabe, T.; Saito, K.; Yamada, T.; Kimura, T. *Opt. Commun*. **2005**, *246*, 229.

(20) Xie, A.; He, Q.; Miller, L.; Sclavi, B.; Chance, M. *Biopolymers* **1999**, *49*, 591.

(21) Gallot, G.; Jamison, S. P.; McGowan, R. W.; Grischkowsky, D. *J. Opt. Soc. Am. B* **2000**, *17*, 851−863.

(22) Mendis, R. R.; Grischkowsky, D. *Opt. Lett.* **2001**, *26*, 846−848.

(23) Zhang, J.; Grischkowsky, D. *Opt. Lett.* **2004**, *19*, 1617.

(24) Laman, N.; Sree Harsha, S.; Grischkowsky, D.; Melinger, J. S. *Biophys. J.* **2007**, accepted for publication.

(25) Ferraris, J. J.; Cowan, D. O.; Walatka, V., Jr.; Perlstein, J. H. *J. Am. Chem. Soc*. **1973**, *95*, 948.

(26) Janczak, J.; Kubiak, R. *Acta Crystallogr., Sect. C: Cryst. Struct. Commun.* **1995**, *51*, 1399−1401; Janczak, J.; Kubiak, R. *J. Mol. Struct*. **2000**, *553*, 157−166.

(27) Carlone, C.; Cyr, C.; Jandl, S.; Hota, N. K.; Zauhar, J. *J. Chem. Phys*. **1982**, *77*, 4920.

(28) White, K. M.; Brose, K.-H.; Eckhardt, C. J. *J. Chem. Phys*. **1986**, *85*, 5551−5559.

(29) van Exter, M.; Grischkowsky, D. *IEEE Trans. Microwave Theory Tech.* **1990**, *38*, 1684−1691.

(30) Laman, N.; Grischkowsky, D. *Appl. Phys. Lett*. **2007**, *90*, 122115.

(31) Lunelli, B.; Pecile, C. *J. Chem. Phys*. **1970**, *52*, 2375.

(32) Esenturk, O.; Heilweil, E. J. *Chem. Phys. Lett*. **2007**, *442*, 71−77.

(33) Carlone, C.; Lemieux, M. A.; Deslandes, J.; Jandl, S.; Truong, K. D.; Hota, N. K.; Zauhar, J. *Can. J. Phys.* **1984**, *62*, 562.

(34) Hess, L. A.; Prasad, P. N. *J. Chem. Phys*. **1980**, *72*, 573−579.

(35) Dlott, D. *Annu. Rev. Phys. Chem.* **1986**, *37*, 157.

(36) Long, R.; Sparks, R. A.; Trueblood, K. N. *Acta Crystallogr*. **1965**, *18*, 932−939.

(37) *Mercury*, version 1.5; Cambridge Crystallographic Data Center: Cambridge, UK.

(38) Briseno, A.; Aizenberg, J.; Han, Y.-J.; Penkala, R. A.; Moon, H.; Lovinger, A. J.; Kloc, C.; Bao, Z. *J. Am. Chem. Soc.* **2005**, *127*, 12164.